CrossMark

Green and yellow luminescence properties of Willemite Zn_2SiO_4 nanocomposites by sol–gel method

J. El Ghoul[1,2]

Abstract

Nanoparticles of willemite, α-Zn_2SiO_4 have been prepared by a sol–gel method. These samples were prepared by a simple solid-phase reaction under natural atmosphere at 1200 °C after the incorporation of ZnO:Mn and ZnO:V nanoparticles in silica monolith. The nanophosphors powder samples were characterized using X-ray diffraction, transmission electron microscopy (TEM) and photoluminescence (PL) spectroscopy. XRD analysis revealed that the α-Zn_2SiO_4 phase was at 1200 °C. In addition, the PL spectrum for the α-Zn_2SiO_4:Mn nanocomposite showed that a dominant peak at 525 nm which is due to $^4T_1$–$^6A_1$ transitions of Mn^{2+} ions. In the case of α-Zn_2SiO_4:V, the PL had shown a band centered around 540 nm. This band is due to the V in the interfaces between Zn_2SiO_4 particles and SiO_2 host matrix. The findings of this work are very promising and can justify the use of these novel materials as a potential candidate in the field of photonic applications.

1 Introduction

Recently, inorganic phosphors are some of the most fundamental materials that support modern society with their wide application in lighting devices; plasma display panels (PDPs) and fluorescent lamps [1–3]. Given the fact that Zn_2SiO_4 material is characterized with high luminescence efficiency and high chemical and physical stability [2, 3], this inorganic phosphors type had become a potential candidate in the industry as phosphor material for plasma display panels.

Hence, it is quite interesting to prepare nano-scaled phosphor to improve the dispersion and luminescence properties [3]. Additionally, nano-scaled phosphor materials offer the potential for preparing a nanocomposite with high luminescence efficiency [1, 3, 4].

For the five past years, the Transition Metal (TM) ions excited state dynamics study in the nanoscale environment had attracted important researcher community interest thanks to the promising optical properties of transition metal ions and nanoparticles.

Furthermore, the material optical properties should be considered in order to get high efficient luminescent processes with an adjustable emission ranging from the ultraviolet (UV) to the infrared (IR) spectral range, including all the visible spectral range [5]. The zinc silicate family is highly versatile material as evident from the properties of α-Zn_2SiO_4, which has the possibility of being a multicolor phosphor by inserting various guest ions instead of Mn^{2+} ions, such as Ga^{3+} for violet-emission, Ce^{3+} or Eu^{2+} for blue-emission, and Eu^{3+} for red-emission as discussed in depth in a review [6–9]. Recently, several studies demonstrated challenging PL properties of Zn_2SiO_4 containing different rare earth and transition metal; Zhang et al. [10] and Hsieh et al. [11] had identified the Zn_2SiO_4:Mn^{2+} and Zn_2SiO_4:Tb^{3+} materials as a phosphor materials which could emit intense green light at 520 and 543 nm, respectively. Kong et al. [12] had prepared Zn_2SiO_4:Mn/SiO_2 spherical core–shell phosphor particles with the green emission at 521 nm. Traditionally, this phosphor is prepared by the solid-state reaction method, which involves a pulverizing process and subsequent high-temperature firing [13]. The resultant Zn_2SiO_4 powder phosphors can be used as paints [14]. Nevertheless, reliable intensity cannot be obtained using these methods. This limitation is explained by the fact that there is inhomogeneous distribution of activator ions, phase separation and impurities contamination [15].

✉ J. El Ghoul
  ghoultn@yahoo.fr

1 Laboratory of Physics of Materials and Nanomaterials Applied at Environment (LaPhyMNE), Faculty of Sciences in Gabes, Gabes University, 6072 Gabes, Tunisia

2 Departement of Physics, College of Sciences, Al Imam Mohammad Ibn Saud Islamic University (IMSIU), Riyadh 11623, Saudi Arabia

Recently, an increasing number of work shad addressed different synthetic procedures for this phosphor; i.e. hydrothermal method [16] polymer pyrolysis [17] and sol–gel method [2, 18]. The sol–gel method has been confirmed to be the most efficient technique in lowering the firing temperature, distributing the activator ions homogeneously and improving the emission efficiency for the powder phosphors [2, 10]. The aim of this work is the use of new protocols for nanoparticles synthesis by the sol–gel technique suitable for various chemical and physical applications [14, 18]. The main objective of this work is to increase the life of components and prevent contamination caused by the external environment by the in-situ synthesis of a luminescent nanoparticles of Zn_2SiO_4 in a silica matrix. This paper is structured as fellows; the second section presents the preparation of zinc silicate nanophosphor using simple sol–gel routes, the third section shows the effects of the doping with Mn and V transition metals on the structural, morphological, optical properties of prepared nanophosphors.

2 Experimental

2.1 Experimental preparation

In order to obtain a luminescent nanocomposites, we have prepared colloid suspension transition metals doped ZnO nanoparticles in a silicate host matrix using a three steps method. In the first one, nanoparticles aerogel were prepared by a sol–gel method using 16 g of zinc acetate dehydrate as precursor in a 112 ml of methanol. After magnetic stirring at room temperature, the appropriate amount of manganese or vanadium acetate was added, and the solution was placed in an autoclave and dried under supercritical conditions of ethyl alcohol. In the second step, we have injected the ZnO nanoparticles in silica aerogel according to the following process: Firstly, 0.5 ml of TEOS is dissolved in EtOH. Then, after a constantly stirring of the mixture TEOS and EtOH, we add 0.44 ml of water and 30 mg of ZnO powder, prepared in the first step. The whole solution is stirred for about 30 min, resulting in the formation of a uniform sol. The obtained sol is transferred then to tube in an ultrasonic bath, where 100 ml of fluoride acid is added. The wet gel formed in few seconds. Monolithic and white aerogel was obtained by supercritical drying in EtOH as described in the first step. Finally, silica glasses containing Zn_2SiO_4:Mn and Zn_2SiO_4:V particles were obtained after firing aerogel at high temperature. In the present case, the thermal treatment was carried out in an oven under natural atmosphere. The aerogel was put into a furnace and heated up to the densification temperature at a heating rate of 50 °C/h. After this step, we performed a heat treatment in air at 1200 °C for 2 h in order to obtain the nanocomposites. The densification

temperature selected (1200 °C) was lower than the fusion temperature of glasses and the formation of macrofissures did not occur. The density achieved at increasing temperature shows two transitions: the first one situated near 700 °C was attributed to the disappearance of the micropores and small mesopores in the aerogel where as the second one located at 1200 °C was attributed to the final densification to glass with a density of about 2 [18–20].

2.2 Characterizations

The crystalline phases of annealed samples were identified by X-ray diffraction (XRD) using a Bruker D5005 powder X-ray diffractometer using a CuKα source (1.5418 Å radiation). Crystallite sizes were estimated from the Scherrer's Equation [21].

$$G = \frac{0.9\lambda}{B\cos\theta_B} \tag{1}$$

where λ is the X-ray wavelength ($\lambda = 1.5418$ Å), θ_B is the maximum of the Bragg diffraction peak (rad) and B is the line width at half maximum.

Transmission electron microscopy (TEM) had been carried out using the JEM-200CX transmission electron microscope in order to study the morphology and the particle size of the phosphor powders. The samples for TEM were prepared by putting the as-grown products in EtOH and immersing them in an ultrasonic bath for 15 min, then dropping a few drops of the resulting suspension containing the synthesized materials onto TEM grid. For photoluminescence (PL) measurements, the 450-W Xenon lamp was used as an excitation source. The sample emitted light was collected by an optical fiber located on the same side as the excitation source and was analyzed with a Jobin–Yvon Spectrometer HR460 using a multichannel CCD detector with a resolution of 2000 pi. The photoluminescence excitation (PLE) measurements were performed on a Jobin–Yvon Fluorolog 3-2 spectrometer. The low temperature experiments were carried out in a Janis VPF-600 Dewar with variable temperature controlled between 78 and 300 K.

3 Results and discussion

3.1 Structural studies

The XRD spectra of undoped, Mn and V-doped ZnO nanopwder have been presented in Fig. 1. All the diffraction peaks of ZnO, ZnO:Mn and ZnO:V samples could be fitted with the hexagonal wurtzite structure(space group P63mc) (No.186) (JCPDS No. 36–1451) [2, 20]. The XRD pattern of our samples indicates the formation of phase ZnO [19,
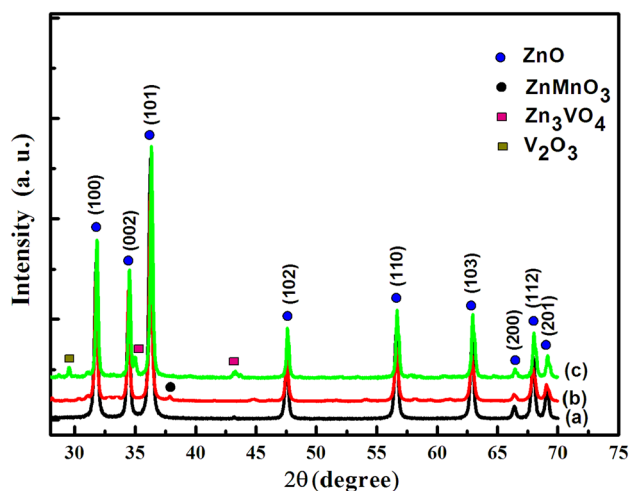
Fig. 1 X-ray diffraction pattern of the (*a*) undoped ZnO, (*b*) ZnO:Mn and (*c*) ZnO:V nanoparticles

Fig. 2 X-ray diffraction pattern of the (*a*) SiO_2/Zn_2SiO_4:Mn and (*b*) SiO_2/Zn_2SiO_4:V nanocomposite

20].In the case of ZnO:Mn, the diffraction peaks of ZnO were found to shift to a smaller angle by Mn doping indicating a increase in the lattice constants [22]. It is known that the ionic radius of Zn^{2+} is smaller than that of Mn^{2+}, so the XRD patterns indicate that the divalent Mn^{2+} ions substitute for Zn^{2+} ions in ZnO crystal lattice and do not change the wurtzite structure [2, 19]. After doping of ZnO with vanadium, in addition to the peaks corresponding to ZnO, four secondary additional phases were detected which can be attributed to V_2O_3 and $Zn_3(VO_4)$ (JCPDS Card 37-1485) [20, 23]. Diffraction lines of ZnO were broad, and diffraction broadening was found to be dependent on the Miller indices of the corresponding sets of crystal planes. For our samples, the (002) diffraction line was more narrower than the (101) line, and the latter one was more narrower than the (100) line. This indicated an asymmetry in the crystallite shape. Average grain size of the crystallites of our samples varies from 18 to 30 nm [18, 19], has been estimated using Scherrer's Formula (1).

The XRD pattern of theSiO₂/ZnO:Mn and SiO₂/ZnO:V nanocomposites treated at 1200 °C for 2 h in air is presented in Fig. 2. These spectra clearly confirm the formation of phase Zn_2SiO_4. In the case of SiO₂/ZnO:Mn nanocomposites it is clear all the diffraction peaks are in good agreement with those of the standard pattern reported by the Joint Committee on Power Diffraction Standard (JCPDS No. 37-1485) [2, 24]. The difference in the peak intensity and width shows that the seeded sample has a higher degree of crystallinity (Fig. 2a). The lattice constants calculated from the XRD pattern are a = 13.944 Å and c = 9.314 Å, which are very close to willemite α-Zn_2SiO_4 [2, 24, 25]. This result confirms that α-Zn_2SiO_4 has a rhombohedral structure [24].Hence, the crystalline phase is the most dominant case corresponding to the α-phase Zn_2SiO_4. Figure 2a highlights also the
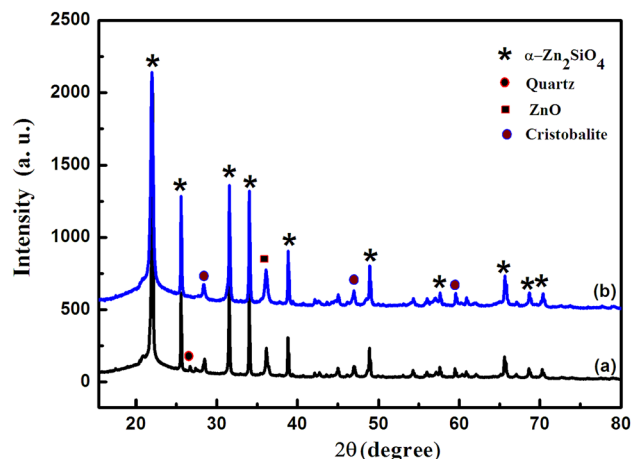
appearance of three other phases that correspond to ZnO, cristobalite and quartz [2, 26]. After incorporation of these nanoparticles ZnO:V in SiO_2, the willemite (α-Zn_2SiO_4) crystals were well developed(Fig. 2b). The lattice constants calculated from the XRD pattern are a = 13.935 Å and c = 9.299 Å, which are very close to willemite α-Zn_2SiO_4 ones, i.e., a = 13.940 Å and c = 9.309 Å [2, 25]. This result indicates that Zn_2SiO_4:V nanocomposite has a rhombohedral structure (JCPDS Card 08-0492).The peak signatures of zinc oxide and cristobalite crystallized phase of silica were also observed with the absence of quartz phase. With respect to our previous results [20, 23], vanadium in hexagonal ZnO results in the improvement of the silica crystallization. However, at high temperature, vanadium doped zinc silica phase was formed when surficial species; i.e. Zn, V and Si move and diffuse inside the porous body. Nevertheless, by the fact that hexagonal zinc oxide and willemite Zn_2SiO_4 coexist in the composite, the solid reaction at higher temperature will not be complete and thus, the obtained composite will be formed by very small ZnO nanoparticles covered by willemite Zn_2SiO_4 as a shell supported by SiO_2 (host matrix).The average grain size of the crystallites Zn_2SiO_4 can be calculated using the Scherrer's formula in Eq. (1) and sizes range from 50 nm to 80 nm. These results bear a close resemblance with Jiang et al. findings [24] for an average Zn_2SiO_4 particle size equal to 100 nm.

The TEM images corresponding to ZnO:Mn (Fig. 3a) and ZnO:V (Fig. 3b) show that the size of the majority of ZnO particles in this powder varied between 15 and 30 nm in good agreement with the results of crystallite size obtained by Debye–Sherrer formula. The TEM micrographs of the SiO₂/Zn_2SiO_4:Mn and SiO₂/Zn_2SiO_4:V nanocomposites treated at 1200 °C for 2 h in air are shown in Fig. 4. At high temperature(~ 1200 °C), Zn and Si species move and diffuse inside the porous body to form Zn_2SiO_4:Mn phase
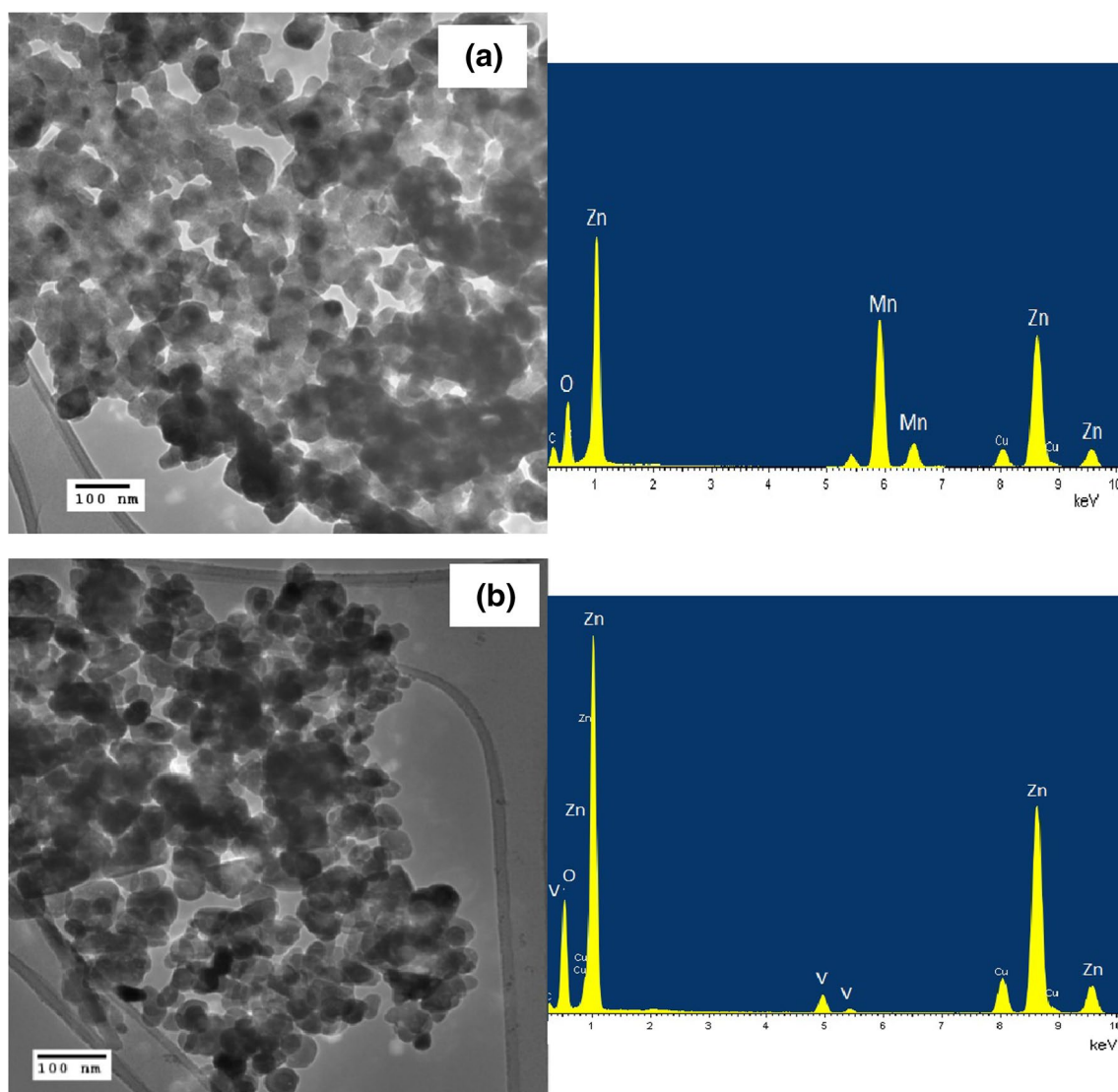
Fig. 3 Typical TEM photograph showing the general morphology and the EDX analysis of nanoparticles: ZnO:Mn (**a**) and ZnO:V (**b**)

with a particle size greater than 80 nm (Fig. 4a). In the case of Zn_2SiO_4:V colloid suspension is formed in silica host matrix with a particle size of about 70 nm (Fig. 4b). Energy dispersive spectroscopy (EDX) analysis during the TEM observation, shown in Figs. 3 and 4, confirm the presence of doping elements. These results are in good agreement with the XRD outcome.

3.2 Photoluminescence studies

The PL spectra of the composites obtained by the 290 nm excitation wavelength consist on a very intensive emission bands located in the visible range. In this section, the intensity and the peak energy dependencies of this PL band versus temperature and power excitation density was studied. The intensity of these luminescence bands observed decreases as the temperature increases. On the other hand, the emission intensity shows a linear variation with the power excitation at high values using 337.1 nm nitrogen laser excitation wavelengths. Furthermore, no change in the PL peaks positions was observed with power excitation and temperature measurement. The shape and the energy location of the PL emission bands are characteristic for a deep levels emission.

Figure 5 shows the PL spectra at different temperatures of measurement and PLE spectrum detected at 525 nm at 78 K for the SiO_2/Zn_2SiO_4:Mn nanocomposite. The PL spectra shown that the SiO_2/Zn_2SiO_4:Mn nanocomposites synthesized by sol–gel method exhibited bright green luminescence (525 nm). As electronic transition of $^4T_1(^4G) \rightarrow {}^6A_1(^6S)$ peaks at 525 nm, which is a parity forbidden emission transition of Mn^{2+} ions [27], green emission occurs. In general, Zn_2SiO_4 host crystal field affects
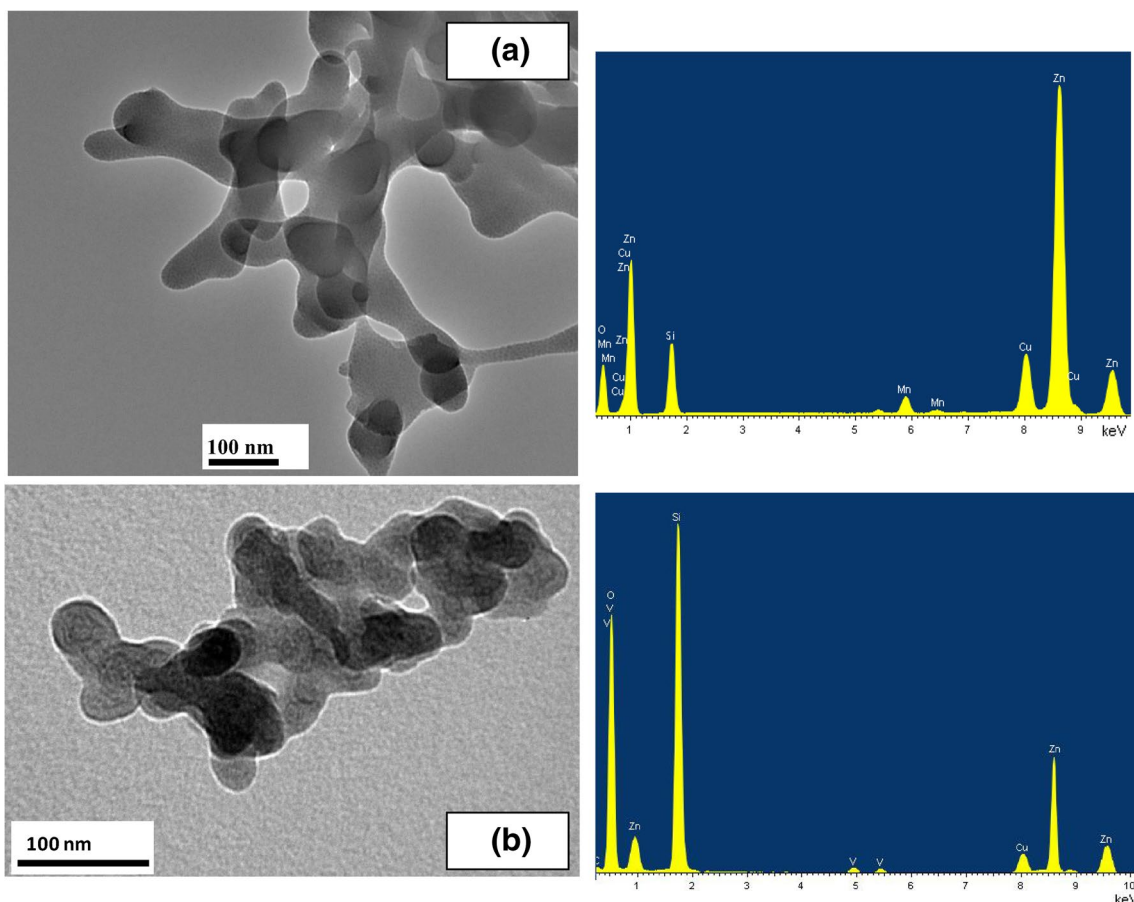
Fig. 4 TEM photograph showing the general morphology and the EDX analysis of the nanocomposites: SiO_2/Zn_2SiO_4:Mn (**a**) and SiO_2/Zn_2SiO_4:V (**b**)
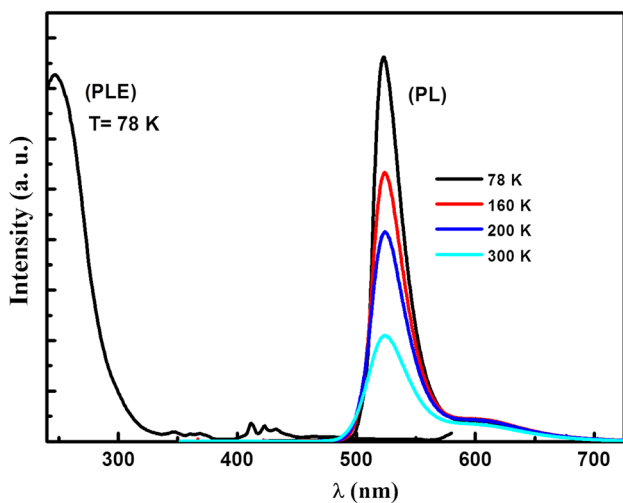

Fig. 5 PLspectra at different temperatures and PLE spectrum detected at 525 nm of a typical SiO_2/Zn_2SiO_4:Mn nanocomposite

the luminescence of Mn^{2+} ion. Mn^{2+} ions in the Zn_2SiO_4 host with higher crystallinity feel a stronger crystal field. By increasing the crystal field, the energy difference of the ground and first excited state decreases, resulting in emission peak broadening and red-shift [14]. This emission centered at 525 nm corresponds to the d–d transition of Mn^{2+} through energy transfer from Zn_2SiO_4 [3, 28] in which Mn^{2+} occupies part of the Zn^{2+} sites, which is coordinated by four oxygen atoms [27]. The SiO_2/Zn_2SiO_4:Mn nanocomposites PLE spectrum detected at 525 nm and at a measurement temperature T = 78 K, shows a strong excitation band ranging from 240 to 300 nm with a maximum at about 255 nm (4.9 eV) with respect to the UV–Vis range bands. Emission at 525 nm is due to the band at 255 nm [29]. The spectra fully agree with previously measured excitation spectrum of Zn_2SiO_4:Mn [29, 30].The broad excitation peak at 255 nm could be attributed to a charge transfer transition (or the ionization of manganese) from the divalent manganese ground state (Mn^{2+}) to the conduction band (CB) [27, 31]. Other bands (inset) of Mn^{2+} (d–d) transitions, caused by crystal field splitting of the ^4D and ^4G levels as shown by the Orgel

diagram for Mn^{2+}, are also observed at higher wavelengths (350–500 nm) in addition to the CT band [8, 32]. The electrons in the $^6A_1$ (^6S) ground state of Mn^{2+} ions, are excited to the conduction band of Zn_2SiO_4 by photons, and the free electrons in the conduction band relax back to the $^4T_1$ (^4G) excited state through a non-radiative process [33]. Finally, this is followed by a radiative transition from the $^4T_1$ (^4G) excited state to the $^6A_1$ (^6S) ground state, giving rise to a green emission band (525 nm).

In the case of the SiO_2/Zn_2SiO_4:V nanocomposite, the PL spectra at different temperatures of measurement and a PLE spectrum detected at 525 nm at 78 K are illustrated in Fig. 6. The PL spectra obtained consists on a very intensive emission band located in the green-yellow spectral range centered at 540 nm. Nine very broad emission bands appear between 1.80 and 2.76 eV with vibrational progressing of $\Delta\gamma = 970$ cm^{-1} corresponds to the transitions from the lowest vibrational level of the excited triplet state $T_1(V^{4+} - O^-)$ to the various vibration levels of the ground state $S_0(V^{5+} = O^{2-})$ [20, 34]. The PLE spectrum of the SiO_2/Zn_2SiO_4:V nanocomposite detected at 540 nm at the measurement temperature T = 78 K shows the appearance of the same band as before, with a maximum at about 250 nm (Fig. 6). This excitation band is essentially due to the Zn_2SiO_4 lattice charge transfer (CT) [2, 8]. The second peak happens at 300 nm and is mainly related to the vanadyl groups charge transfer. One can note that this mechanism is strongly affected by both ligand field strength and V^{5+} species interference along with oxygen vacancies [20, 35].

Figures 7 and 8 present the intensity and the peak energy dependence of the PL band versus power excitation density of these nanocomposites. The emission intensity of two nanocomposites showed a linear variation with the excitation power. Furthermore, no change in the PL spectra, neither
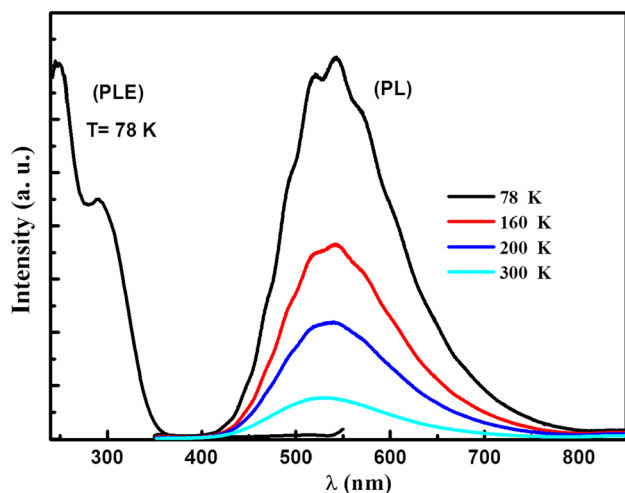

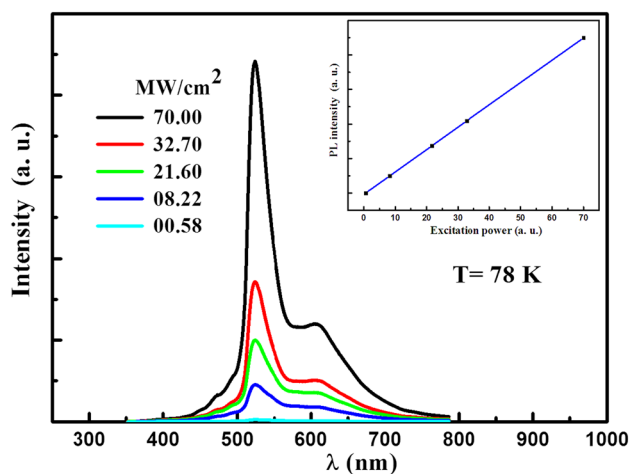**Fig. 7** The variation of the PL intensity with the power excitation density at the UV range of the SiO_2/Zn_2SiO_4:Mn nanocomposite. The inset shows the linear variation of PL intensity

the shape nor position, was observed with power excitation, even after being aged for a longue period of time, indicating the time stability of the composite material. For doping with Mn, the conventional green luminescence is there of SiO_2/α-Zn_2SiO_4:Mn^{2+} nanocomposite, occurring at about 525 nm, a well-known, it corresponds to an internal transition of Mn^{2+} in α-Zn_2SiO_4 phase and the second bands in the range 560–608 nm for Mn^{2+} in the β-Zn_2SiO_4 phase [24, 25]. Also, the strong emissions peaks around 525 and 590 nm are observed only under the highest excitation power density 70 MW/cm^2 (Fig. 7). The sharpness of the peak can be ascribed as due to the uniformity of particle sizes. In the case of doping with vanadium, two strong and sharp

Fig. 6 PL at different temperatures and PLE spectrum detected at 540 nm of a typical SiO_2/Zn_2SiO_4:V nanocomposite

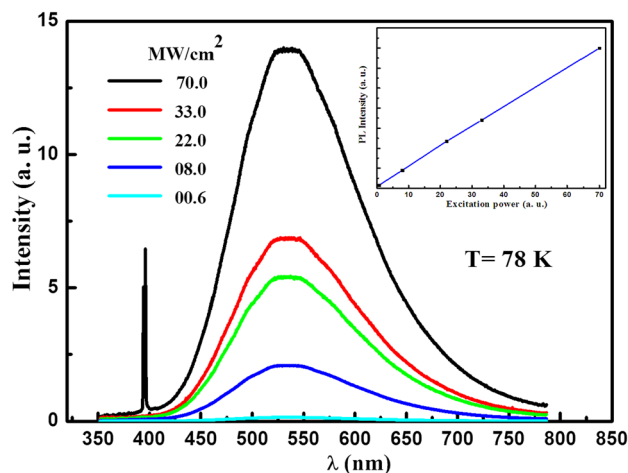**Fig. 8** The variation of the PL intensity with the power excitation density at the UV range of the SiO_2/Zn_2SiO_4:V nanocomposite. The inset shows the linear variation of PL intensity

emission peaks around 394 and 396 nm are observed only under the highest excitation power density 70 MW/cm^2 in parallel of more similar to those of Mn behavior (Fig. 8). The shape of these peaks is similar to those recently reported in V-implanted zinc oxide nanorods [26], and are likely to be due to donor–acceptor pairs (DAP) recombination. The absence of these emissions for lower excitation power range, confirms XRD results. This mean that the solid reaction at higher temperature is not completed and the obtained composite is formed by very few and small ZnO nanoparticles covered by willemite Zn_2SiO_4 as a shell supported by SiO_2 as a host matrix. Thus, the PL-related to dopant element in zinc oxide which covered by willemite and supported by silica can be observed only under very intensive power excitation of UV-light. This result strongly suggests that an energy transfer occurs from Zn_2SiO_4 particles to radiative defects attributed to presence of V^{5+} in the interfaces between willemite particles and SiO_2 host matrix. Under very high power excitation these levels are saturated and the recombination can be observed from donor–acceptor pairs in ZnO.

4 Conclusion

This work presents a successfully effort on the willemite Zn_2SiO_4 nano powders synthesis. The structural and optical properties of these novel materials are widely studied; the X-ray diffraction and TEM of Mn and V-doped ZnO nanoparticles show a crystalline phase with a particle size ranging between 18 and 30 nm. Upon incorporation of ZnO:Mn and ZnO:V nanoparticles in SiO_2 and heat treatment at 1200 °C, Zn_2SiO_4 phase was formed in SiO_2 host matrix. The PL spectra of the SiO_2/Zn_2SiO_4:Mn nanocomposite showed a strong green luminescence band located at 525 nm. This emission can be attributed to Mn^{2+}inZn_2SiO_4 particle.In the other hand, the PL spectrum for the SiO_2/Zn_2SiO_4:V showed that a dominant peak at 540 nm appears, which is due to the V^{5+} ions present in the interfaces between Zn_2SiO_4 particles and SiO_2 host matrix.PL measurements as a function of the power excitation is static and no change was observed, even after being aged for a longue period of time. This indicates that composite material is timely stabilite.

References

1. Z. Li, H. Zhang, H. Fu, J. Luminesc **135**, 79 (2013)
2. J. El Ghoul, K. Omri, L. El Mir, C. Barthou, S. Alaya, J. Luminesc **132**, 2288 (2012)
3. P. Thiyagarajan, M. Kottaisamy, M.S. Ramachandra Rao, Scr. Mater. **57**, 433 (2007)
4. W.C. Wang, Y.T. Tian, K. Li, E.Y. Lu, D.S. Gong, X.J. Li, Appl. Surf. Sci. **273**, 372 (2013)
5. Y.C. Kanga, S.B. Parka, Mater. Res. Bull. **35**, 1143 (2000)
6. S.R. Lukic, D.M. Petrovic, M.D. Dramicanin, M. Mitric, Lj. Dacanin, Scr. Mater. **58**, 655 (2008)
7. Q. Lu, G. Yun, Ceram. Int. **39**, 3533 (2013)
8. C. Barthou, J. Benoit, P. Benallouland, A. Morell, J. Electrochem. Soc. **141**, 524 (1994)
9. A. Patra, G.A. Baker, S.N. Baker, Opt. Mater. **27**, 15 (2004)
10. H.X. Zhang, S. Buddhudu, C.H. Kam, Y. Zhou, Y.L. Lam, K.S. Wong, B.S. Ooi, S.L. Ngand, W.X. Que, Mater. Chem. Phys. **68**, 31 (2001)
11. H.Y. Hsieh, S.E. Lin, W. Cheng, J. Wei, J. Lumin. **129**, 595 (2009)
12. D.Y. Kong, M. Yu, C.K. Lin, X.M. Liu, J. Lin, J. Fang, J. Electrochem. Soc. **152**, H146 (2005)
13. Q.Y. Zhang, K. Pita, C.H. Kam, J. Phys. Chem. Solids **649**, 333 (2003)
14. X. Li, F. Chen, Mater. Res. Bull **48**, 2304 (2013)
15. C.R. Rondaand, T. Amrein, J. Lumin. **69**, 245 (1996)
16. Q. Lu, P. Wang, J. Li, Mater. Res. Bull. **46**, 791 (2011)
17. K. Su, D.T. Tilley, M.J. Sailor, J. Am. Chem. Soc. **118**, 3459 (1996)
18. J. El Ghoul, K. Omri, A. Alyamani, C. Barthou, L. El Mir, J. Luminesc. **138**, 218 (2013)
19. J. El Ghoul, C. Barthou, L. El Mir, Physica E, **44** 1910. (2012)
20. J. El Ghoul, K. Omri, S.A. Gómez-Loperaand, L. El Mir, Opt. Mater. **36** 1034 (2014)
21. B.D. Cullity, *Elements of X-ray Diffractions* (Addison-Wesley, Reading, MA, 1978), p. 102
22. S. Chakraborty, C.S. Tiwary, A.K. Kole, P. Kumbhakar, K. Chattopadhyay, Mater. Lett. **91**, 379 (2013)
23. J. El Ghoul, C. Barthou, L. El Mir, Superlattices Microstruct., **51** 942 (2012)
24. Y. Jiang, J. Chen, Z. Xie, L. Zheng, J. Mater. Chem. Phys. **120**, 313 (2010)
25. M. Takesue, H. Hayashi, R. Lee Smith Jr., J. Prog. Cryst. Growth Charact. Mater. **55**, 98 (2009)
26. J. El Ghoul, C. Barthou, M. Saadoun, L. El, Mir, J. Phys. Chem. Solids **71**, 194 (2010)
27. R. Selomulya, S. Ski, K. Pita, C.H. Kam, Q.Y. Zhang, S. Buddhudu, J. Mater. Sci. Eng. B **100**, 136 (2003)
28. N. Taghavinia, G. Lerondela, H. Makino, A. Yamamoto, T. Yao, Y. Kawazoe, T. Goto, J. Nanotechnol. **12**, 547 (2001)
29. M. Mai, C. Feldmann, Solid State Sci. **11**, 528 (2009)
30. D.J. Robbins, N.S. Casewell, Ph. Avouris, E.A. Giess, I.F. Chang, D.B. Dove, J. Electrochem. Soc. **132**, 2784 (1985)
31. K.S. Sohn, B. Cho, H.D. Park, J. Am. Ceram. Soc. **82**, 2779 (1999)
32. L.E. Orgel, J. Chem. Phys. **23**, 1004 (1955)
33. L. Xiong, J. Shi, J. Gu, L. Li, W. Huang, J. Gao, M. Ruan, J. Phys. Chem. B **109**, 731 (2005)
34. M. Anpo, S. Higashimoto, M. Matsuoka, N. Zhanpeisov, Y. Shioya, S. Dzwigaj, M. Che, Catal. Today **78**, 211 (2003)
35. G. Gao, R. Meszaros, M. Pengand, L. Wondraczek, Opt. Express **19**, A312 (2011)